J. Am. Soc. Mass Spectrom. (2018) 29:2380–2393
DOI: 10.1007/s13361-018-2065-0

RESEARCH ARTICLE

Sequence Ion Structures and Dissociation Chemistry of Deprotonated Sucrose Anions

Benjamin J. Bythell,[1] Jordan M. Rabus,[1] Ashley R. Wagoner,[1] Maha T. Abutokaikah,[1] Philippe Maître[2]

[1]Department of Chemistry and Biochemistry, University of Missouri St. Louis, St. Louis, MO 63121, USA
[2]Laboratoire de Chimie Physique (UMR8000), CNRS, Univ. Paris-Sud, Université Paris-Saclay, 91405, Orsay, France

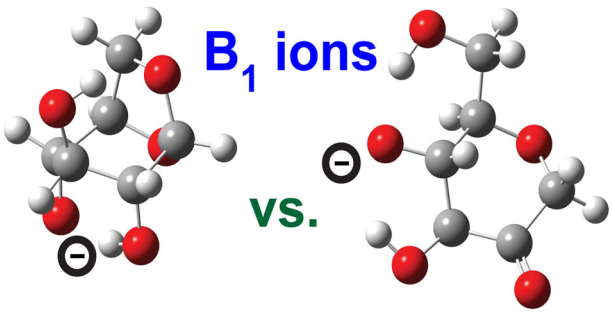

Abstract. We investigate the tandem mass spectrometry of regiospecifically labeled, deprotonated sucrose analytes. We utilize density functional theory calculations to model the pertinent gas-phase fragmentation chemistry of the prevalent glycosidic bond cleavages (B_1-Y_1 and C_1-Z_1 reactions) and compare these predictions to infrared spectroscopy experiments on the resulting B_1 and C_1 product anions. For the C_1 anions, barriers to interconversion of the pyranose [α-glucose-H]$^-$, C_1 anions to entropically favorable ring-open aldehyde-terminated forms were modest (41 kJ mol^{-1}) consistent with the observation of a band assigned to a carbonyl stretch at ~ 1680–1720 cm^{-1}. For the B_1 anions, our transition structure calculations predict the presence of both deprotonated 1,6-anhydroglucose and carbon 2-ketone ((4S,5S,6R)-4,5-dihydroxy-6-(hydroxymethyl)dihydro-2H-pyran-3(4H)-one) anion structures, with the latter predominating. This hypothesis is supported by our spectroscopic data which show diagnostic bands at 1600, 1674, and 1699 cm^{-1} (deprotonated carbon 2-ketone structures), and at ~ 1541 cm^{-1} (both types of structure) and RRKM rate calculations. The deprotonated carbon 2-ketone structures are also the lowest energy product B_1 anions.
Keywords: Carbohydrates, Collision-induced dissociation, Density functional theory, IRMPD

Received: 6 August 2018/Revised: 6 September 2018/Accepted: 6 September 2018/Published Online: 3 October 2018

Introduction

Complex carbohydrates (glycans) contain a wealth of biological information. Over half of the proteins in the human body are glycosylated [1] with cells presenting a multitude of glycan structures [2]. Glycan biomarkers are present in all body fluids, on cell surfaces, within cells, and in many diseases [3–8]. Changes in the level of glycans and in branching patterns can indicate presence and progression of a disease [9, 10]. Consequently, fast, accurate, and highly sensitive identification tools for these important analytes are highly desirable [3, 11–19]. Tandem mass spectrometry-based approaches [11, 12, 14–22] coupled with liquid and/or gas-phase separations [15, 19, 23–30] are commonly utilized to achieve this goal. However, the combination of the gigantic number of compositional isomers of the precursor ions and any fragments generated, with low sample abundance of precursor ions and their inherent lability make accurate molecular determination a challenging task.

Additionally, the lack of an obvious, universally effective method of glycan sequencing and structural identification [31, 32] has led to a substantial increase in the number and type of analyses performed with the goal of remedying this difficulty. The expansion in breadth and range of techniques reflect the diversity of analyses undertaken and the current need to tailor approaches to the specific analyte classes. In the present paper, we investigate one such approach, namely analysis of

Electronic supplementary material The online version of this article (https://doi.org/10.1007/s13361-018-2065-0) contains supplementary material, which is available to authorized users.

Correspondence to: Benjamin Bythell; *e-mail:* bythellb@umsl.edu

deprotonated, negatively charged carbohydrates [33–36]. Analysis of deprotonated carbohydrates has shown the potential for isomer discrimination due to gas-phase structure [27] and/or fragmentation characteristics [19, 33, 34, 36–38]. Despite this potential, deprotonated carbohydrate anions are relatively under-investigated from a fundamental dissociation chemistry perspective [36, 39, 40], particularly in comparison to recent cationized systems [41–47].

Here we present some of our initial mechanistic investigations into the complex gas-phase fragmentation chemistry of deprotonated carbohydrate anions. To accomplish this task, we utilize regiospecific labelling, tandem mass spectrometry, and computational chemistry. To provide additional, rigorous testing of our structural hypotheses, we then utilize wavelength selective infrared multiple photon dissociation (IRMPD) action spectroscopy to further characterize the B_n and C_m product anions (Chart 1 [48]). Gas-phase spectroscopy of carbohydrates and carbohydrate fragments has recently been utilized to provide alternate, complementary analyses of gas-phase carbohydrate ions [25, 29, 39, 49–55]. In principle, spectroscopy coupled to mass spectrometry offers the potential means of distinguishing isomeric precursors or fragment ions based on their IR 'fingerprint'. Such an approach offers the potential of identifying or at very least disambiguating carbohydrates and/or their fragments effectively.

Experimental Methods

Experimental spectroscopic work was carried out in a Fourier transform-ion cyclotron resonance (FT-ICR) mass spectrometer (Bruker Apex IV Qe, Bremen, Germany) [56]. Labeled and unlabelled $[sucrose–H]^-$ anions were sprayed under conventional electrospray conditions. Low-energy collisional activation and subsequent thermalization of the generated fragment ions is achieved in a linear hexapole pressurized with Ar at $\sim 10^3$ mbar. Fragment ions of interest are then pulse-extracted into the ICR cell where they are mass-selected and subsequently irradiated with IR light. IR spectroscopy was carried out using the free-electron laser (FEL) at the Centre Laser Infrarouge d'Orsay (CLIO) [57, 58]. For each analyte, we follow all the precursor ion and fragment ion peaks. For the m/z 161.047 ($C_6H_9O_5$), B_1 anion, the fragment peaks were m/z 143.036 ($C_6H_7O_4$) and 113.025 ($C_5H_5O_4$); for the m/z 179 ($C_6H_{11}O_6$), C_1 anion, the fragment peaks were m/z 161.047 ($C_6H_9O_5$), 143.036 ($C_6H_7O_4$), 131.035 ($C_5H_7O_4$), 119.036 ($C_4H_7O_4$), 113.025 ($C_5H_5O_4$), and 101.025 ($C_4H_5O_3$). The abundances of these photo fragments and their corresponding precursors were recorded as a function of the IR wavelength in order to derive the IR action spectra where the IRMPD efficiency is plotted against the photon energy. Both the IR FEL power variation and wavelength are monitored online while recording the IRMPD spectrum. For this purpose, a small fraction of the IR beam is directed towards a power meter. A second power meter is used to record the IR absorption spectrum of a polystyrene film using a second fraction of the IR FEL beam. As a result, at each wavelength during the IR FEL scan, relative power, polystyrene absorption, and a mass spectrum are simultaneously recorded. Wavelength and power corrections can thus be made during the data treatment.

Regioselectively, $^{13}C_6$-labeled sucrose samples α-D-glucopyranosyl-(1 → 2)-β-D-$^{13}C_6$-fructofuranoside were purchased from Omicron Biochemicals, Inc. (South Bend, IN, USA). Standard sucrose and labeled sucrose standards were prepared for MS analysis in water/methanol solution (50/50) at a concentration of 50 μM.

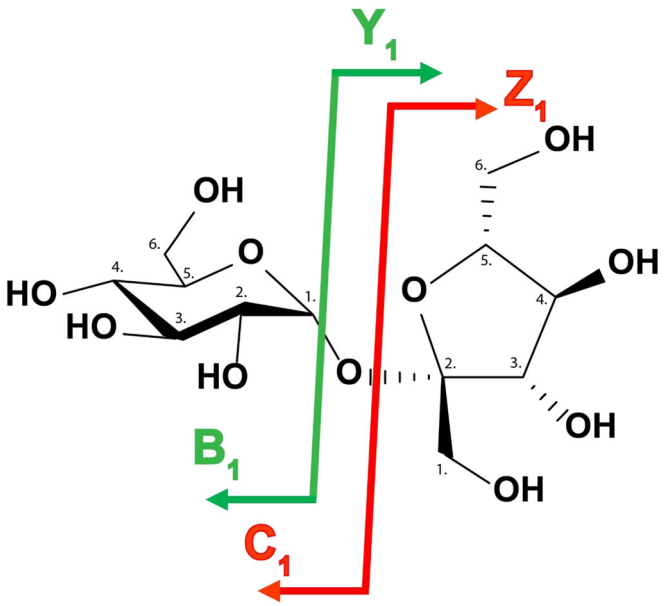

Chart 1. Carbohydrate fragmentation nomenclature of Domon and Costello [48] illustrated for sucrose

Theoretical Methods

Simulations were performed to enable effective characterization of the potential energy surface of all analytes. Initial candidate structures for deptotonated sucrose as well as multiple potential fragment anions were systematically generated via the tool Fafoom [59–61], a genetic algorithm with the generated structures initially optimized using the MMFF94 Force Field [62–66]. Geometry optimizations of the resulting candidate conformations were performed with the Gaussian 09 software package [67] at the B3LYP/6-31++G(d,p) [68–70], then M06-2X/6-31++(d,p) [71, 72] levels of theory. Degenerate structures were removed, and the non-degenerate structures were utilized as the starting points of subsequent refinement. Analogous density functional theory optimizations of neutral conformations generated in Fafoom were also utilized as the starting points for generation of anion structures by scripts that removed a single hydroxyl proton. Optimizations of these putative anion structures were performed at the HF/3-21g, M06-2X/6-31G(d), and then M06-2X/6-31++(d,p) levels of theory with degenerate structures removed after each stage. The resulting (pooled) non-degenerate structures were re-optimized at the B3LYP/6-311++(2d,2p) level of theory with single point calculations performed at the M06-2X/6-311++(2d,2p), and MP2/6-311++(2d,2p) [73] levels of theory to assess energetic variability as a function of model and basis set. Density functional theory calculations of minima, transition structures, product ions, and neutrals present on each potential reaction pathway were performed at the M06-2X/6-31++G(d,p) level of theory. Multiple transition structures (TSs) were systematically generated and calculated from multiple precursor ion structures for each potential fragmentation pathway. Minima and TSs were tested by vibrational analysis (all real frequencies or one imaginary frequency, respectively). The potential energy surface generated combines the zero-point energy correction (ZPE) to the electronic energy (E_{el}, 0 K) for improved accuracy ($\Delta E_{el+ZPE,0\ K}$). The related, standard enthalpy ($\Delta H_{298\ K}$), Gibbs free energy ($\Delta G_{298\ K}$), and entropy ($\Delta S_{298\ K}$) corrections to 298 K were also determined. The reaction pathway through each TS was determined by intrinsic reaction coordinate (IRC) calculations with up to ten steps in each direction. The terminating points of these calculations (one on product-side, one on reactant-side) were then optimized further to determine which minima were connected to each TS. Calculated B3LYP/6-311++(2d,2p) vibrational frequencies were utilized for comparisons with the experimental IRMPD spectra. A 20 cm^{-1} full width at half maximum Gaussian line shape and a scaling factor of 0.967 was utilized for the vibrational frequencies for comparison to the experimental spectra.

Rice–Ramsperger–Kassel–Markus (RRKM) calculations were performed using the energetics, vibrational frequencies, and rotational constants derived from the modeling to approximate the time scale of the fragmentation reactions [74, 75]. The Beyer–Swinehart direct count algorithm [76] was used for rotational–vibrational treatment of both the reactant and the transition structure.

Results and Discussion

Tandem Mass Spectrometry

Our FT-ICR tandem mass spectra of [α-D-glucopyranosyl-(1 → 2)-β-D-$^{13}C_6$-fructofuranoside-H]$^-$ generate an abundant C_1 anion peak with a lower abundance B_1 anion peak at low collision energies (Fig. 1). At increased collision energies, consecutive losses and/or cross-ring cleavages from the glucose end of the precursor anion become increasingly prevalent.

[Sucrose-H]$^-$ Minima

The lowest energy conformers of [sucrose-H]$^-$ are predicted to have a proton bridged between the glucose carbon 2, secondary hydroxyl oxygen and the fructose carbon 1, primary hydroxyl oxygen, with the former as the ostensive site of deprotonation (alkoxide, Fig. 2). A range of hydrogen-bonding patterns and

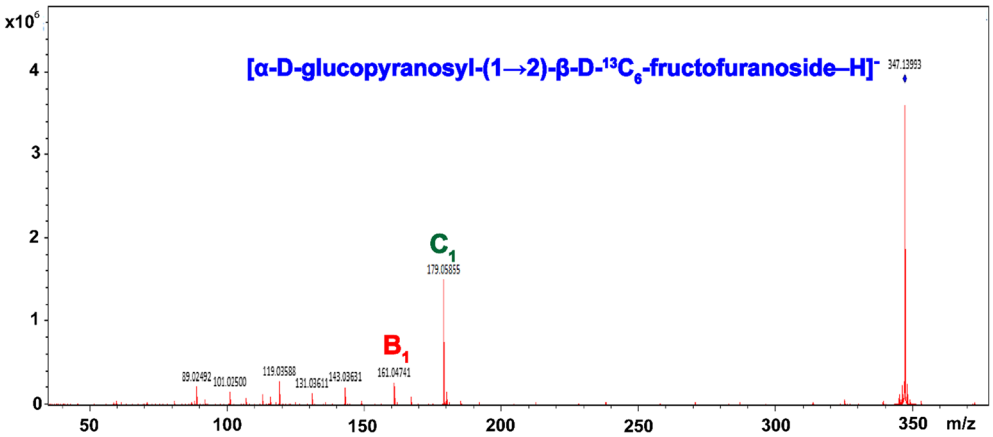

Figure 1. Example FT-ICR MS/MS spectrum of regioselectively labelled, deprotonated sucrose, [α-D-glucopyranosyl-(1 → 2)-β-D-$^{13}C_6$-fructofuranoside-H]$^-$

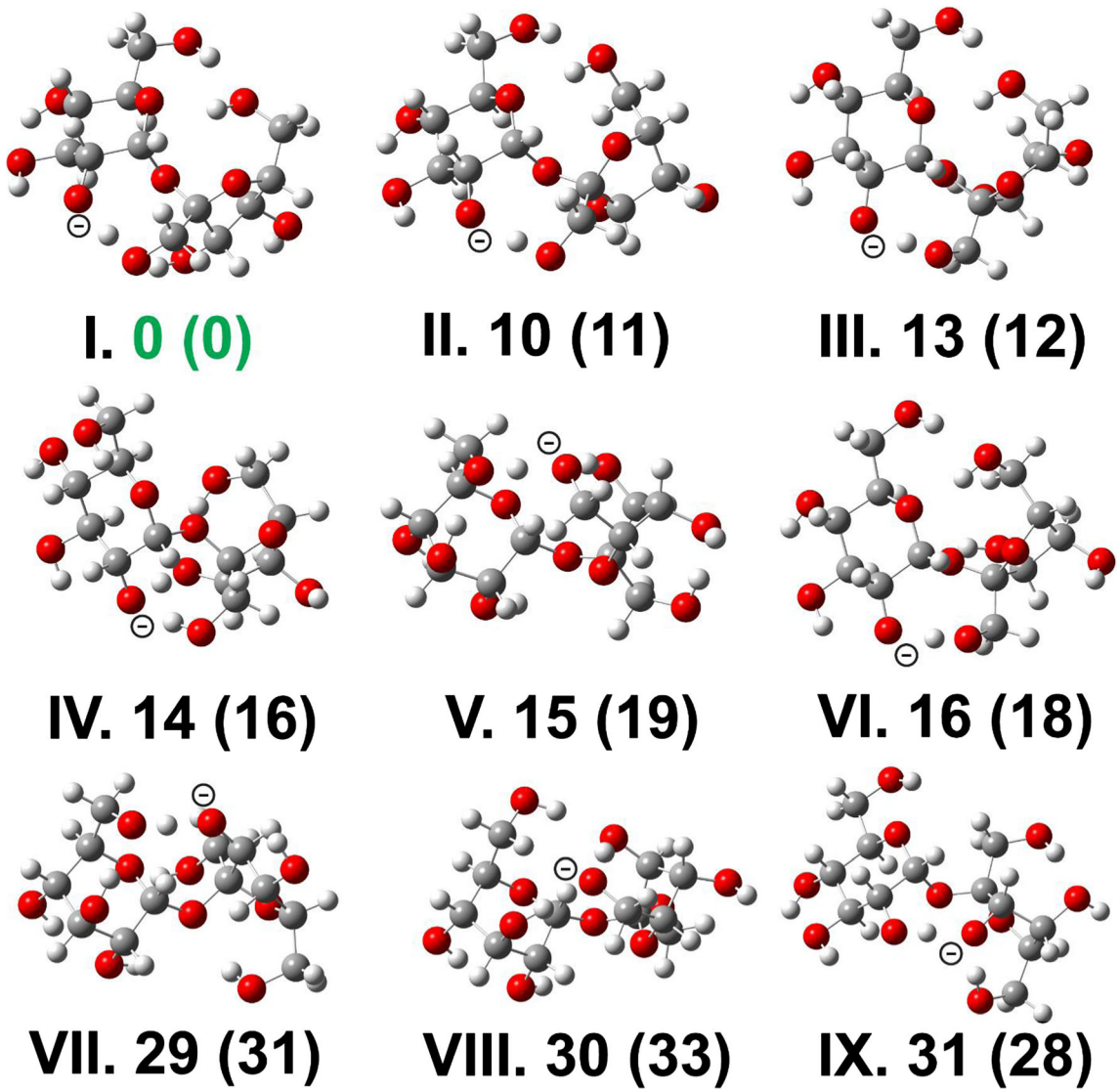

Figure 2. Relative energies of six lowest energy low-energy conformers of deprotonated sucrose and selected higher energy conformers calculated at the M06-2X/6-31++G(d,p) level of theory. Values in kJ mol^{-1}: $\Delta E_{el+ZPE,0\ K}$ (ΔG_{298}). The site of deprotonation (alkoxide site) is indicated in each case for illustration

ring deformations provide differing degrees of stabilization to these structures. At least 15 kJ mol^{-1} is required to enable population of alternate sites of deprotonation (structure V, Fig. 2). Our calculations predict deprotonation of the fructose carbon 6 primary hydroxyl to be the next most readily accessible site. This structure is stabilized by hydrogen bonds from both the glucose primary hydroxyl and the fructose carbon 3 secondary hydroxyl protons. Other structures deprotonated at

Table 1. Relative energies of the minima, transition structures, and product anions and neutrals of deprotonated sucrose (α-D-glucopyranosyl-(1 → 2)-β-D-fructofuranoside) calculated at the M06-2X/6-31++G(d,p) level of theory

Structures	E_{el}/H	E_{el+ZPE}/H	$\Delta E_{el+ZPE,0\ K}$/kJ mol^{-1}	ΔH_{298}/kJ mol^{-1}	ΔG_{298}/kJ mol^{-1}	ΔS_{298}/J K^{-1} mol^{-1}
Global minimum	− 1296.998483	− 1296.636443	0	0	0	0
B_1-Y_1 TS (1,6-anhydroglucose)	− 1296.930470	− 1296.568129	179.4	178.1	180.3	− 7.2
B_1-Y_1 TS (carbon 2-ketone)	− 1296.918015	− 1296.562194	194.9	196.6	190.4	20.6
C_1-Z_1 TS_A (1,2-anhydrofructose)	− 1296.936071	− 1296.574242	163.3	161.4	164.5	− 10.5
C_1-Z_1 TS_B (1,2-anhydrofructose)	− 1296.927728	− 1296.566876	182.6	184.4	178.4	20.0
1,6-anhydroglucose, B_1+D-fructose	− 1296.930026	− 1296.569262	176.4	175.5	120.2	185.5
carbon 2-ketone, B_1+D-fructose	− 1296.940551	− 1296.583070	140.1	142.9	78.5	215.9
[α-glucose-H]$^-$, C_1+1,2-anhydrofructose	− 1296.920738	− 1296.560822	198.5	198.7	139.9	197.3
Ring-open aldehyde, C_1+1,2-anhydrofructose	− 1296.915531	− 1296.558661	204.2	208.2	139.3	231.2

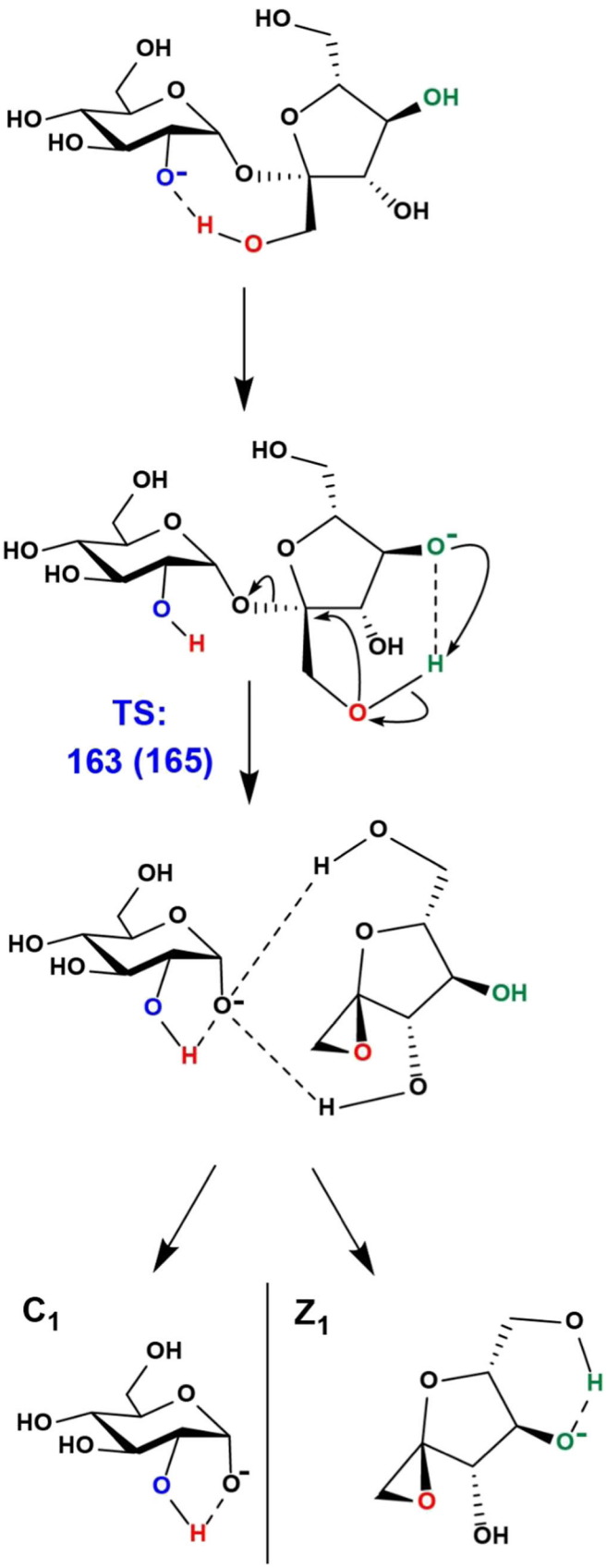

Scheme 1. The lowest-energy C_1-Z_1 glycosidic bond cleavage pathways of deprotonated sucrose; formation of deprotonated α-D-glucose C_1 anions and/or deprotonated 1,2-anhydrofructose Z_1 anions. Values in kJ mol^{-1}: $\Delta E_{el+ZPE,0\ K}$ (ΔG_{298})

the fructose carbon 6 primary hydroxyl are possible, but predicted to be less energetically favorable (VIII and IX, Fig. 2). However, these structure types are important in the B_1 and C_1 anion-forming mechanisms. Population of fructose, carbon 3 hydroxyl deprotonated structures and other sites are predicted to require more than 29 kJ mol^{-1} (VII, Fig. 2).

C_1-Z_1 Glycosidic Bond Cleavage Reactions and Product Anions

Both the lowest energy calculated transition structures (Table 1) and our regioselectively labeled spectra (Fig. 1) support the C_1-Z_1 reaction producing C_1 anion peaks, as the most facile glycosidic bond cleavage process. Initially, collisional activation enables proton transfers and rotations (Scheme 1) which result in structure X (Fig. S1, 34 (37) kJ mol^{-1}: $\Delta E_{el+ZPE,0\ K}$ (ΔG_{298})) which is deprotonated at the fructose carbon 4 secondary hydroxyl with solvation by the fructose carbon 1 primary hydroxyl proton. The fructose carbon 4 primary alkoxide abstracts the solvating proton enabling nucleophilic attack of the newly formed fructose carbon 1 primary alkoxide group into fructose carbon 2 which causes cleavage of the glycosidic bond and formation of a dimer comprising [α-glucose-H]$^-$ and 1,2-anhydrofructose (Scheme 1). The lowest energy transition structure located (C_1-Z_1 TS_A, Table 1, Fig. 3a) is predicted to require at least 163 (165) kJ mol^{-1}. Separation of the dimer yields a C_1 anion, [α-glucose-H]$^-$ and requires at least 199 (140) kJ mol^{-1}. Consequently, an alternative, mechanistically highly similar, but entropically substantially preferred transition structure (C_1-Z_1 TS_B, $\Delta S_{298} = 20$ J K^{-1} mol^{-1}, Table 1, Fig. 3b) is likely to be competitive too. Both reactions yield the same product dimer components.

Our C_1 anion infrared action spectrum is shown in Fig. 4. Consistent with the prior literature [39,] there are substantial bands at ~1700 cm^{-1}. These bands are inconsistent with pyranose [α-glucose-H]$^-$ structures (Fig. 4d–f, Fig. S2a) as there are no absorptions predicted between 1550 and 1900 cm^{-1}. This broad feature is consistent with the assignment of aldehyde carbonyl stretches present in the entropically favored ring-open isomers (Fig. 4a–c, Fig. S2) where this stretch is predicted to occur at ~1700 cm^{-1}. We calculated the barriers to ring-opening to generate aldehyde-terminated isomers from multiple deprotonated α-D-glucopyranose C_1 conformers. This process is readily achievable with the lowest of many low-energy barriers at just 41 (39) kJ mol^{-1} (Scheme 2). The lower energy parts of the spectrum are less diagnostic. Of the ring-open aldehyde structures, the two lowest energy structures (Fig. 4b, c) are more consistent with experiment than Fig. 4a or the low-energy pyranose structures. However, the breadth (and potential overlap) of the experimental bands makes discounting the possibility of some glucopyranose population impossible (despite the lack of a pyranose-diagnostic band in the wavelength range examined). For example, the lowest energy (< 1240 cm^{-1}) part of the spectrum has intense spectral features, predicted to correspond to hydrogen-bonded,

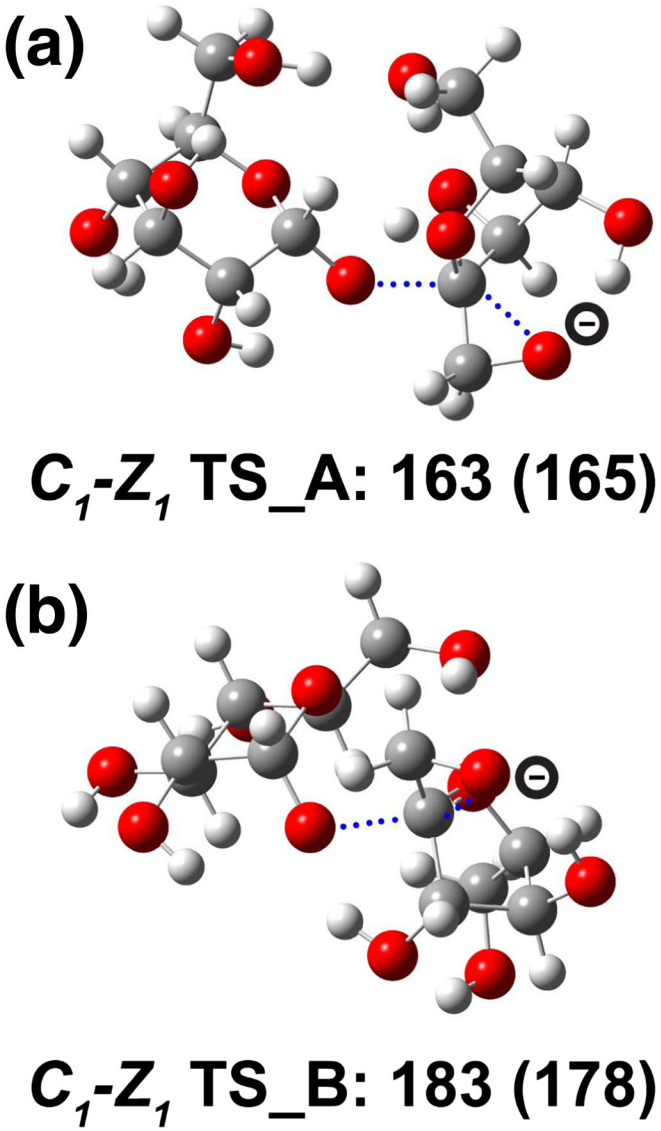

Figure 3. Deprotonated sucrose lowest energy C_1-Z_1 TSs calculated at the M06-2X/6-31++G(d,p) level of theory. **(a)** C_1-Z_1 TS_A and **(b)** C_1-Z_1 TS_B. Values in kJ mol^{-1}: $\Delta E_{el+ZPE,0\ K}$ (ΔG_{298}). The site of deprotonation (alkoxide site) is indicated in each case for illustration. Blue dotted lines show the glycosidic bond that is cleaved and the incoming nucleophiles

primary hydroxide C-O$^-$ stretch coupled to O-H bends. These bands are predicted for both pyranose and ring-open aldehyde structures at similar frequencies. This is also consistent with the earlier literature. [39].

B_1-Y_1 Glycosidic Bond Cleavage Reactions and Product Anions

The situation for the B_1-Y_1 fragmentation reaction is more complex than for the C_1-Z_1 pathway. Production of B_1 anion peaks is predicted to occur most readily by forming either deprotonated 1,6-anhydroglucose B_1 or carbon 2-ketone B_1 anion structures (Scheme 3, Table 1). The former reaction is enthalpically preferred whereas the latter is substantially more entropically

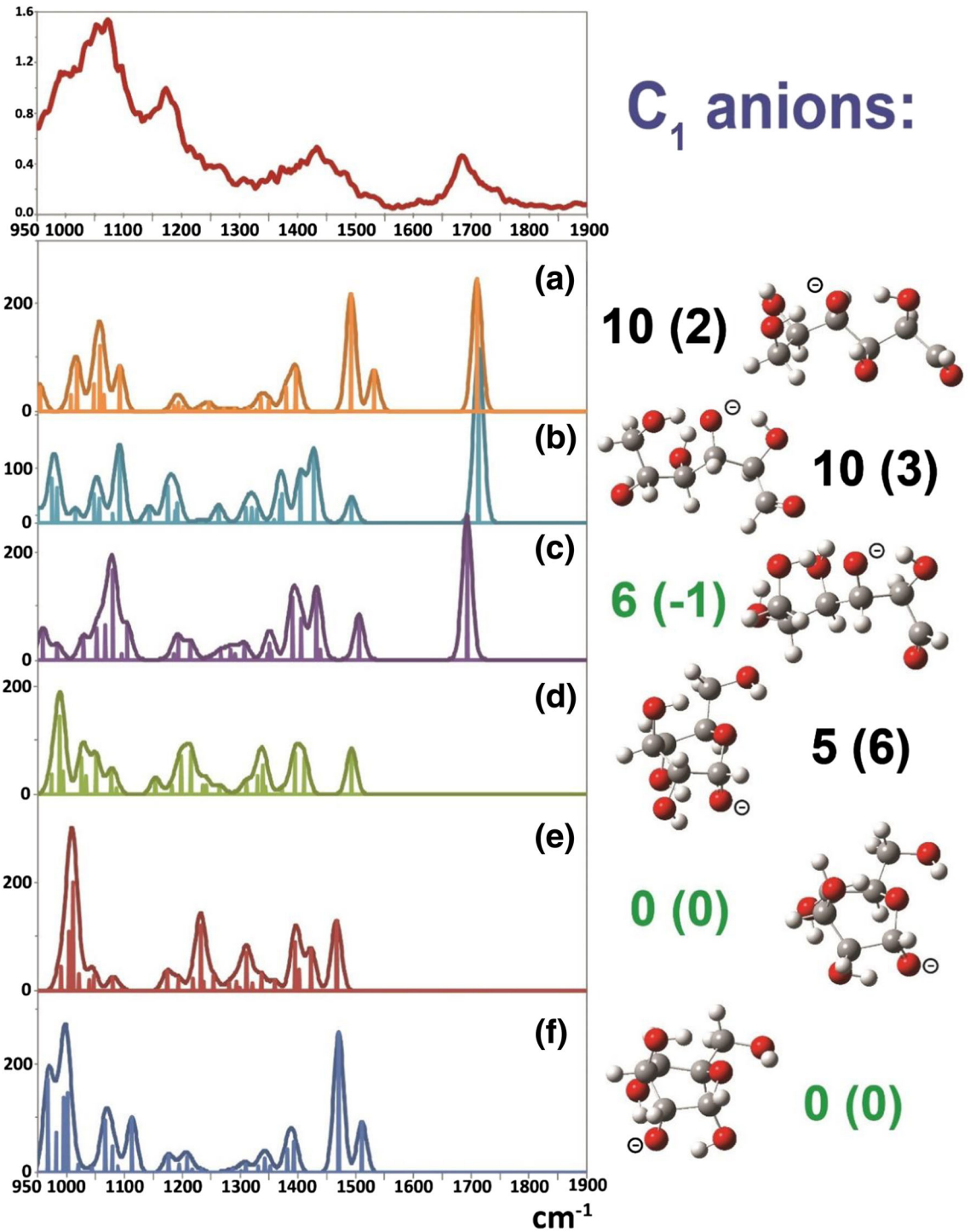

Figure 4. C_1 anion infrared action spectrum compared to the lowest energy structural possibilities with frequencies calculated from B3LYP/6-311++G(2d,2p) optimized structures. Panels **(a–c)**: Ring-open deprotonated glucose structures; panels **(d–f)**: [α-glucose-H]$^-$. Relative energies calculated at the M06-2X/6-31++G(d,p) level of theory. Values in kJ mol^{-1}: $\Delta E_{el+ZPE,0\ K}$ (ΔG_{298})

favorable. The deprotonated 1,6-anhydroglucose B_1 anion-forming pathway begins with proton transfers and rotations which enable population of a reactive configuration (structure XI, 38 (39) kJ mol^{-1}: $\Delta E_{el+ZPE,0\ K}$ (ΔG_{298}), Fig. S3) deprotonated at the carbon 6 primary hydroxyl of glucose. Concerted nucleophilic attack by the carbon 6 alkoxide into the adjacent carbon 1 in an S_N2-like reaction simultaneously cleaves the glycosidic bond (B_1-Y_1 TS_A, 179 (180) kJ mol^{-1}, Fig. 5, Scheme 3a, Table 1) and produces a dimer of 1,6-anhydroglucose and deprotonated fructose. Proton transfer to the fructose anion followed by dimer separation enables detection of a deprotonated 1,6-anhydroglucose B_1 anion (Fig. S4). The alternate, lowest

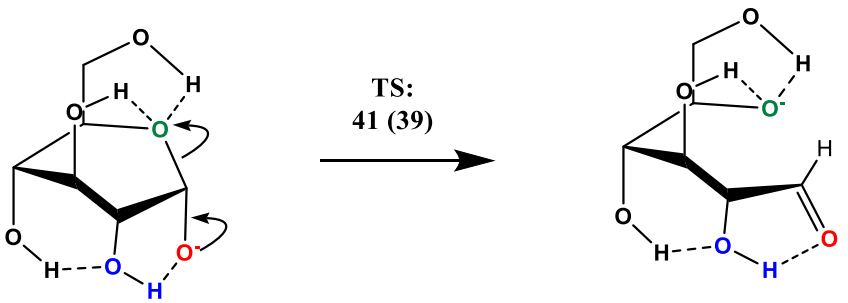

Scheme 2. Facile ring-opening isomerization of deprotonated α-D-glucose C_1 anion structure. Values in kJ mol^{-1}, $\Delta E_{el+ZPE,0\ K}$ (ΔG_{298})

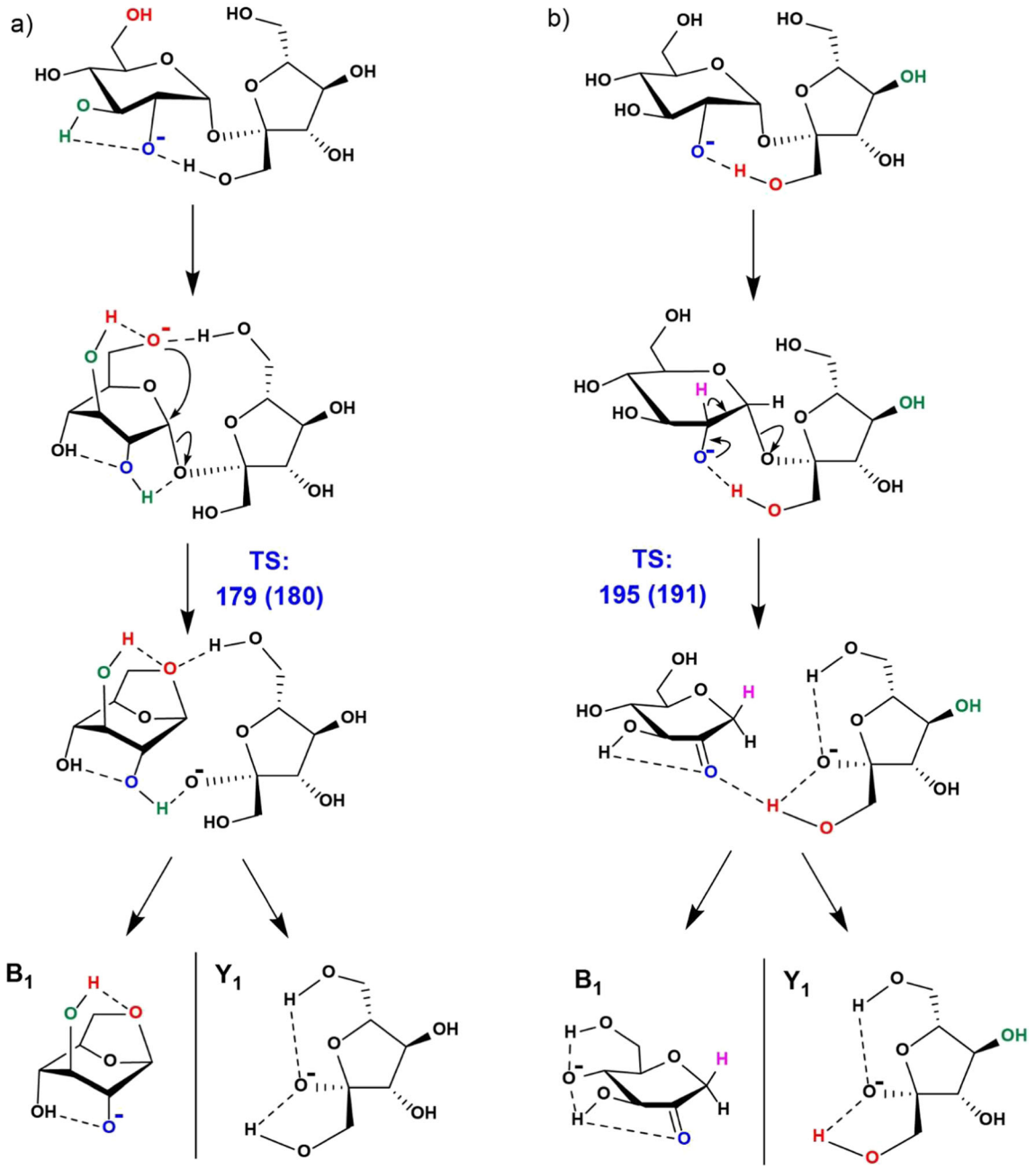

Scheme 3. The lowest-energy B_1-Y_1 glycosidic bond cleavage pathways of deprotonated sucrose; **(a)** formation of deprotonated 1,6-anhydroglucose B_1 anion and **(b)** formation of deprotonated ketone B_1 anion. Both reactions alternatively produce a deprotonated D-fructose Y_1 anion. Values in kJ mol^{-1} $\Delta E_{el+ZPE,0\ K}$ (ΔG_{298})

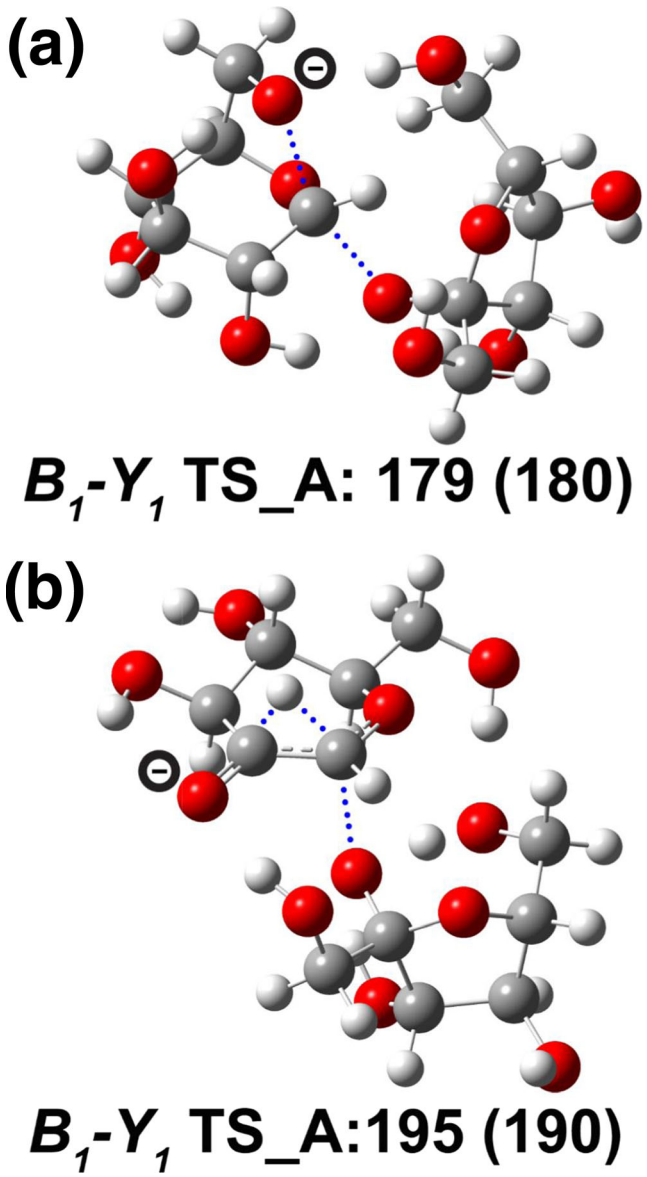

Figure 5. Deprotonated sucrose lowest energy B_1-Y_1 TSs calculated at the M06-2X/6-31++G(d,p) level of theory. **(a)** B_1-Y_1 TS (1,6-anhydroglucose) and **(b)** B_1-Y_1 TS (carbon 2-ketone). Values in kJ mol^{-1}: $\Delta E_{el+ZPE,0\ K}$ (ΔG_{298}). The site of deprotonation (alkoxide site) is indicated in each case for illustration. Blue dotted lines show the glycosidic bond that is cleaved and the incoming nucleophiles

energy carbon 2-ketone B_1 anion-forming B_1-Y_1 fragmentation pathway involves ketone formation, combined with a hydride shift from glucose carbon 2 to carbon 1 (the anomeric carbon), and glycosidic bond cleavage (B_1-Y_1 TS_B, 195 (190) kJ mol^{-1}, Fig. 5b, Scheme 3b, Table 1) in a concerted reaction which produces a dimer comprising a carbon 2-ketone structure and deprotonated fructose. Again, proton transfer to the fructose anion followed by dimer separation enables detection of the B_1 anion (deprotonated carbon 2-ketone, Fig. S4). Both of these reaction pathways are kinetically controlled. We also investigated many routes to the deprotonated 1,2-anhydroglucose B_1 product structures invoked in some of the early carbohydrate literature. These are not supported by our transition structure calculations as the calculated barriers substantially exceed (≥ 263 (260) kJ mol^{-1}) the previously discussed pathways. Nevertheless, we compared the theoretical spectra calculated from these hypothetical product anions to the experimental data.

Our B_1 anion IRMPD spectrum is shown in Fig. 6. This spectrum provides evidence for the deprotonated 1,6-anhydroglucose and carbon 2-ketone anion (deprotonated (4S,5S,6R)-4,5-dihydroxy-6-(hydroxymethyl)dihydro-2H-pyran-3(4H)-one) structures indicating that the dissociation conditions enable populations of both analytes. The lowest energy deprotonated carbon 2-ketone B_1 anion structures have diagnostic bands predicted at higher energies (> 1550 cm^{-1}) than do the deprotonated anhydroglucose forms. We assign the experimental band at ~ 1600 cm^{-1} to the lowest energy carbon 2-ketone B_1 anion structure (Fig. 6b, 1601 cm^{-1}); predicted to be a vibration involving the

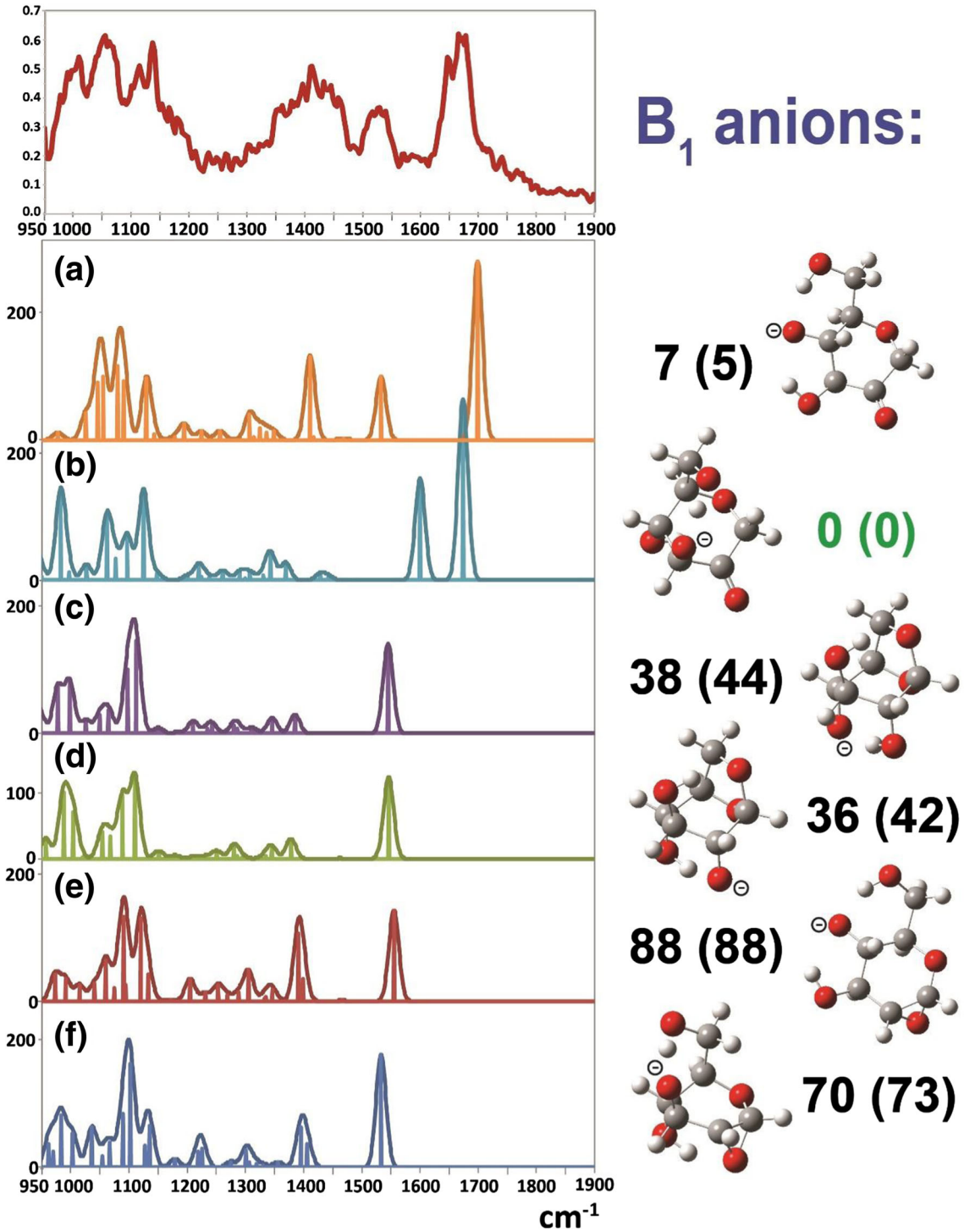

Figure 6. B_1 anion infrared action spectroscopy spectrum compared to the lowest energy structural possibilities with frequencies calculated from B3LYP/6-311++G(2d,2p) optimized structures. Panels **(a)** and **(b)**: deprotonated ketone structures; panels **(c)** and **(d)**: [1,6-anhydroglucose-H]$^-$ structures; panels **(e)** and **(f)**: [1,2-anhydroglucose-H]$^-$ structures. Relative energies calculated at the M06-2X/6-31++G(d,p) level of theory. Values in kJ mol^{-1}: $\Delta E_{el+ZPE,0\ K}$ (ΔG_{298})

proton of the carbon 6 hydroxyl group positioned in close proximity to the carbon 3 alkoxide. The proton oscillates up and down in the plane of these two oxygens, rather than back and forth between them (that band is predicted at 2158 cm^{-1} which is well beyond our experimental range). The low energy side of the unresolved experimental feature between 1650 and 1710 cm^{-1} is assigned as the diagnostic ketone-carbonyl stretch (Fig. 6b, 1675 cm^{-1}) predicted by the lowest energy carbon 2-ketone B_1 anion structure. To assign the higher energy part of the experimentally observed feature requires invoking a population of the second lowest energy B_1 anion structure too (Fig. 6a). This structure has a

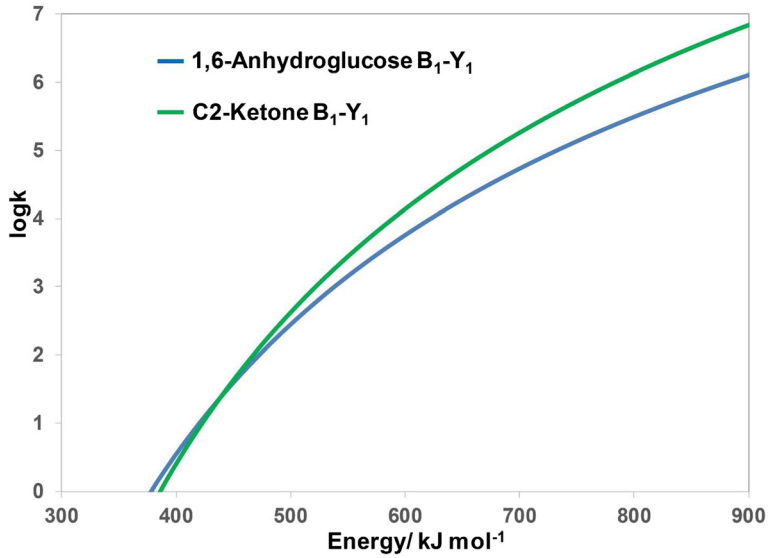

Figure 7. RRKM unimolecular rate constants, k (s^{-1}) calculated at various internal energies for the lowest energy B_1-Y_1 pathways of deprotonated sucrose

diagnostic, higher energy ketone-carbonyl stretch predicted at 1699 cm^{-1} which is consistent with the unresolved spectral feature, i.e., partial overlap of the carbonyl stretches from the two structures producing a broader experimental band. No bands are predicted in this range for either the deprotonated 1,6-anhydroglucose or 1,2-anhydroglucose structural possibilities. In contrast, the next experimental feature is an intense band from ~ 1500 to 1560 cm^{-1} which is found in all of our structural categories (Fig. 6a, c–f). This band is predicted to correspond to a C-O-H bending motion with the hydroxyl proton coordinated to an adjacent alkoxide group. Once again, we detect intense bands below ~ 1500 cm^{-1}. Regrettably, the combination of spectral overlap and the resolution of our experiments make it impossible to discount deprotonated 1,6- or even the 1,2-anhydroglucose anion structures solely based on the spectroscopic data. Formation of the deprotonated 1,6-anhydroglucose B_1 anion structures is supported by our TS calculations with these reactions having the lowest enthalpic barrier (Table 1, Fig. 5a). However, our calculations indicate that formation of deprotonated 1,2-anhydroglucose B_1 anion structures is highly unlikely.

We investigated the potential energetic dependence of the deprotonated 1,6-anhydroglucose and deprotonated carbon 2-ketone B_1 anion-forming reactions further with RRKM unimolecular dissociation rate calculations (Fig. 7). We found additional support for the carbon 2-ketone B_1 anion assignment (green line) as the RRKM data supports this reaction being more competitive than the 1,6-anhydroglucose B_1–Y_1 reaction (blue line) under most experimental conditions. The differences are not especially or uniformly large though, indicating a population of the 1,6-anhydroglucose B_1 anion is entirely reasonable. In summary, our combined experimental and theoretical data support the presence of both deprotonated 1,6-anhydroglucose and carbon 2-ketone B_1 anion structures (Fig. S4).

Alternate Mechanisms and Chemical Models

We examined the effect of basis set and model chemistry on our approach. Larger basis sets containing diffuse functions are typically necessary to adequately describe gas-phase anion energy and thus chemistry accurately relative to their positively charged congeners. Somewhat surprisingly we do not see substantial differences in the relative energies of deprotonated sucrose minima between the quite modest 6-31++G(d,p) basis set calculations performed with the M06-2X functional and the single point calculations with the more substantial M06-2X/6-311++(2d,2p), and MP2/6-311++(2d,2p) methods. The B3LYP/6-311++(2d,2p) calculations show a little more variation, but are also very consistent. Summaries describing the $[sucrose\text{-}H]^-$ ions are provided in Tables S1 and S2. For the important transition structures we also made this same comparison (Table S3). The M06-2X data is highly consistent in both barrier magnitude and relative values between the two basis sets. In contrast, the MP2 single point calculations of the TS barriers result in an approximately 20 kJ mol^{-1} reduction in the computational reaction barrier height estimates for the S_N2-like reactions (1,6-anhydroglucose and 1,2-anhydrofructose forming TSs) relative to the M06-2X data. The B3LYP/6-311++(2d,2p) TS single point calculations result in substantial, systematic lowering of all TS barriers investigated here (30–44 kJ mol^{-1}, Table S3). This finding is not entirely surprising as B3LYP has a documented tendency to underestimate both 1,2-H shift and S_N2 reactions [77–81]. Overall, the general predictions of our TS modeling are consistent over multiple models and basis sets, but the magnitudes of the barriers vary.

Lastly, we note that we also investigated the possibility of ring-opening mechanisms at the non-reducing end of the

precursor anion. These approaches led to barriers that were more energetically demanding than the fragmentation mechanisms described in this manuscript. We note however that these differences are not huge, so this does not preclude these types of reactions from being important for larger carbohydrate anions.

Conclusions

Our combined tandem mass spectrometry, IRMPD spectroscopy, and calculations provide evidence for a mixture of both deprotonated carbon 2-ketone and 1,6-anhydroglucose B_1 anion structures. Formation of the deprotonated carbon 2-ketone structure is entropically favored, but enthalpically disfavored relative to the 1,6-anhydroglucose-forming pathway. At higher degrees of activation, the deprotonated carbon 2-ketone-forming reaction should predominate. We also provide theoretical evidence for formation of pyruvate C_1 anions which then facilely ring-open to generate aldehyde-terminated isomers (barrier only ≥ 41 kJ mol^{-1}). This computational result is consistent with the observation of a band assigned as an aldehyde, with a carbonyl stretch at ~1680–1720 cm^{-1} in our IRMPD spectrum. Consequently, our C_1 anion spectroscopic and theoretical findings offer direct support to the earlier data and interpretation provided by Bendiak and co-authors [39, 40]. Namely, that at very least, a portion of deprotonated monosaccharide and monosaccharide sequence anions exist as ring-open aldehyde-terminated isomers. Subsequent work will address routes to alternate fragment anions generated from other deprotonated carbohydrates and whether the present findings are general.

Acknowledgments

The authors are grateful to E. Loire, J. M. Ortega, F. Gobert, and N. Jestin for technical support. Calculations were performed at the Missouri University of Science and Technology Rolla, MO

Funding Information

This material is based (in part) upon work supported by the National Science Foundation under 1808394 (to BJB) and a 2018 University of Missouri-St. Louis Office of Research Administration Award. Maha T. Abutokaikah thanks the Saudi Arabia Culture Mission for a graduate fellowship. The research leading to this result has been supported by the project CALIPSOplus under the Grant Agreement 730872 from the EU Framework Programme for Research and Innovation HORIZON 2020. Financial Support from the National FT-ICR network (FR3624 CNRS) for conducting the research is gratefully acknowledged.

References

1. Varki, A., Cummings, R.D., Esko, J.D., Freeze, H.H., Stanley, P., Betozzi, C.R., Hart, G.W., Etzler, M.E.: Essentials of Glycobiology. Cold Spring Harbor Laboratory Press, New York (2008)
2. Alonzi, D.S., Neville, D.C.A., Lachmann, R.H., Dwek, R.A., Butters, T.D.: Glucosylated free oligosaccharides are biomarkers of endoplasmic-reticulum alpha-glucosidase inhibition. Biochem. J. **409**, 571–580 (2008)
3. Ruhaak, L.R., Miyamoto, S., Lebrilla, C.B.: Developments in the identification of glycan biomarkers for the detection of cancer. Mol. Cell. Proteomics MCP. **12**, 846–855 (2013)
4. Yin, Z., Huang, X.: Recent development in carbohydrate based anticancer vaccines. J. Carbohydr. Chem. **31**, 143–186 (2012)
5. Adamczyk, B., Tharmalingam, T., Rudd, P.M.: Glycans as cancer biomarkers. Biochim. Biophys. Acta. **1820**, 1347–1353 (2012)
6. Reis, C.A., Osorio, H., Silva, L., Gomes, C., David, L.: Alterations in glycosylation as biomarkers for cancer detection. J. Clin. Pathol. **63**, 322–329 (2010)
7. Huang, Y.-L., Hung, J.-T., Cheung, S.K.C., Lee, H.-Y., Chu, K.-C., Li, S.-T., Lin, Y.-C., Ren, C.-T., Cheng, T.-J.R., Hsu, T.-L., Yu, A.L., Wu, C.-Y., Wong, C.-H.: Carbohydrate-based vaccines with a glycolipid adjuvant for breast cancer. Proc. Natl. Acad. Sci. U. S. A. **110**, 2517–2522 (2013)
8. Fujitani, N., Furukawa, J., Araki, K., Fujioka, T., Takegawa, Y., Piao, J., Nishioka, T., Tamura, T., Nikaido, T., Ito, M., Nakamura, Y., Shinohara, Y.: Total cellular glycomics allows characterizing cells and streamlining the discovery process for cellular biomarkers. Proc. Natl. Acad. Sci. **110**, 2105–2110 (2013)
9. Lebrilla, C.B., An, H.J.: The prospects of glycan biomarkers for the diagnosis of diseases. Mol. BioSyst. **5**, 17–20 (2009)
10. Meany, D.L., Zhang, Z., Sokoll, L.J., Zhang, H., Chan, D.W.: Glycoproteomics for prostate cancer detection: changes in serum PSA glycosylation patterns. J. Proteome Res. **8**, 613–619 (2009)
11. Kailemia, M.J., Ruhaak, L.R., Lebrilla, C.B., Amster, I.J.: Oligosaccharide analysis by mass spectrometry: a review of recent developments. Anal. Chem. **86**, 196–212 (2013)
12. Reinhold, V.N., Reinhold, B.B., Costello, C.E.: Carbohydrate molecular weight profiling, sequence, linkage, and branching data: ES-MS and CID. Anal. Chem. **67**, 1772–1784 (1995)
13. Mirgorodskaya, E., Karlsson, N.G., Sihlbom, C., Larson, G., Nilsson, C.L.: Cracking the sugar code by mass spectrometry: an invited perspective in honor of Dr. Catherine E. Costello, recipient of the 2017 ASMS distinguished contribution award. J. Am. Soc. Mass Spectrom. (2018). https://doi.org/10.1007/s13361-018-1912-3
14. Yu, X., Jiang, Y., Huang, Y., Costello, C.E., Lin, C.: Detailed glycan structural characterization by electronic excitation dissociation. Anal. Chem. **85**, 10017–10021 (2013)
15. Zheng, X., Zhang, X., Schocker, N.S., Renslow, R.S., Orton, D.J., Khamsi, J., Ashmus, R.A., Almeida, I.C., Tang, K., Costello, C.E., Smith, R.D., Michael, K., Baker, E.S.: Enhancing glycan isomer separations with metal ions and positive and negative polarity ion mobility spectrometry-mass spectrometry analyses. Anal. Bioanal. Chem. **409**, 467–476 (2017)
16. Ashline, D.J., Hanneman, A.J.S., Zhang, H., Reinhold, V.N.: Structural documentation of glycan epitopes: sequential mass spectrometry and spectral matching. J. Am. Soc. Mass Spectrom. **25**, 444–453 (2014)
17. Lapadula, A.J., Hatcher, P.J., Hanneman, A.J., Ashline, D.J., Zhang, H., Reinhold, V.N.: Congruent strategies for carbohydrate sequencing. 3. OSCAR: an algorithm for assigning oligosaccharide topology from MSn data. Anal. Chem. **77**, 6271–6279 (2005)
18. Park, Y., Lebrilla, C.B.: Application of Fourier transform ion cyclotron resonance mass spectrometry to oligosaccharides. Mass Spectrom. Rev. **24**, 232–264 (2005)
19. Ashwood, C., Lin, C.-H., Thaysen-Andersen, M., Packer, N.H.: Discrimination of isomers of released N- and O-Glycans using diagnostic product ions in negative ion PGC-LC-ESI-MS/MS. J. Am. Soc. Mass Spectrom. 1–16 (2018). https://doi.org/10.1007/s13361-018-1932-z
20. Khatri, K., Pu, Y., Klein, J.A., Wei, J., Costello, C.E., Lin, C., Zaia, J.: Comparison of collisional and electron-based dissociation modes for middle-down analysis of multiply glycosylated peptides. J. Am. Soc. Mass Spectrom. (2018). https://doi.org/10.1007/s13361-018-1909-y
21. Campbell, M.T., Chen, D., Glish, G.L.: Identifying the D-pentoses using water adduction to lithium cationized molecule. J. Am. Soc. Mass Spectrom. **28**, 1420–1424 (2017)
22. Campbell, M.T., Chen, D., Glish, G.L.: Distinguishing linkage position and anomeric configuration of glucose–glucose disaccharides by water adduction to lithiated molecules. Anal. Chem. **90**, 2048–2054 (2018)

23. Veillon, L., Huang, Y., Peng, W., Dong, X., Cho, B.G., Mechref, Y.: Characterization of isomeric glycan structures by LC-MS/MS. Electrophoresis. **38**, 2100–2114 (2017)
24. Gaye, M.M., Nagy, G., Clemmer, D.E., Pohl, N.L.B.: Multidimensional analysis of 16 glucose isomers by ion mobility spectrometry. Anal. Chem. (2016). https://doi.org/10.1021/acs.analchem.5b04280
25. Gray, C.J., Schindler, B., Migas, L.G., Picmanova, M., Allouche, A.R., Green, A.P., Mandal, S., Motawia, M.S., Sánchez-Pérez, R., Bjarnholt, N., Møller, B.L., Rijs, A.M., Barran, P.E., Compagnon, I., Eyers, C.E., Flitsch, S.L.: Bottom-up elucidation of glycosidic bond stereochemistry. Anal. Chem. **89**, 4540–4549 (2017)
26. Harvey, D.J., Scarff, C.A., Edgeworth, M., Struwe, W.B., Pagel, K., Thalassinos, K., Crispin, M., Scrivens, J.: Travelling-wave ion mobility and negative ion fragmentation of high-mannose N-glycans. J. Mass Spectrom. **51**, 219–235 (2016)
27. Struwe, W.B., Baldauf, C., Hofmann, J., Rudd, P.M., Pagel, K.: Ion mobility of deprotonated oligosaccharide isomers - evidence for gas-phase charge migration. Chem. Commun. **52**, 12353–12356 (2016)
28. Morrison, K.A., Clowers, B.H.: Contemporary glycomic approaches using ion mobility–mass spectrometry. Curr. Opin. Chem. Biol. **42**, 119–129 (2018)
29. Hernandez, O., Isenberg, S., Steinmetz, V., Glish, G.L., Maitre, P.: Probing mobility selected saccharide isomers: selective ion-molecule reactions and wavelength-specific IR activation. J. Phys. Chem. A. **119**, 6057–6064 (2015)
30. Abrahams, J.L., Campbell, M.P., Packer, N.H.: Building a PGC-LC-MS N-glycan retention library and elution mapping resource. Glycoconj. J. **35**, 15–29 (2018)
31. National Research Council (US) Committee on Assessing the Importance and Impact of Glycomics and Glycosciences: Transforming Glycoscience A Roadmap for the Future. National Academic Press, Washington, DC (2012)
32. EGSF, IBCarb Network & European Science Foundation. A Roadmap for Glycosciences in Europe. (2014)
33. Harvey, D.J.: Fragmentation of negative ions from carbohydrates: part 1. Use of nitrate and other anionic adducts for the production of negative ion electrospray spectra from N-linked carbohydrates. J. Am. Soc. Mass Spectrom. **16**, 622–630 (2005)
34. Harvey, D.J.: Fragmentation of negative ions from carbohydrates: part 2. Fragmentation of high-mannose N-linked glycans. J. Am. Soc. Mass Spectrom. **16**, 631–646 (2005)
35. Harvey, D.J.: Fragmentation of negative ions from carbohydrates: part 3. Fragmentation of hybrid and complex N-linked glycans. J. Am. Soc. Mass Spectrom. **16**, 647–659 (2005)
36. Doohan, R.A., Hayes, C.A., Harhen, B., Karlsson, N.G.: Negative ion CID fragmentation of O-linked oligosaccharide aldoses—charge induced and charge remote fragmentation. J. Am. Soc. Mass Spectrom. **22**, 1052–1062 (2011)
37. Wheeler, S.F., Harvey, D.J.: Negative ion mass spectrometry of sialylated carbohydrates: discrimination of N-acetylneuraminic acid linkages by MALDI-TOF and ESI-TOF mass spectrometry. Anal. Chem. **72**, 5027–5039 (2000)
38. Pfenninger, A., Karas, M., Finke, B., Stahl, B.: Structural analysis of underivatized neutral human milk oligosaccharides in the negative ion mode by nano-electrospray MS(n) (part 1: methodology). J. Am. Soc. Mass Spectrom. **13**, 1331–1340 (2002)
39. Brown, D.J., Stefan, S.E., Berden, G., Steill, J.D., Oomens, J., Eyler, J.R., Bendiak, B.: Direct evidence for the ring opening of monosaccharide anions in the gas phase: photodissociation of aldohexoses and aldohexoses derived from disaccharides using variable-wavelength infrared irradiation in the carbonyl stretch region. Carbohydr. Res. **346**, 2469–2481 (2011)
40. Bendiak, B., Fang, T.T.: Assignment of the stereochemistry and anomeric configuration of structurally informative product ions derived from disaccharides: infrared photodissociation of glycosyl-glycolaldehydes in the negative ion mode. Carbohydr. Res. **345**, 2390–2400 (2010)
41. Abutokaikah, M.T., Frye, J.W., Tschampel, J., Rabus, J.R., Bythell, B.J.: Fragmentation pathways of lithiated hexose monosaccharides. J. Am. Soc. Mass Spectrom. (2018). https://doi.org/10.1007/s13361-018-1973-3
42. Rabus, J.M., Abutokaikah, M.T., Ross, R.T., Bythell, B.J.: Sodium-cationized carbohydrate gas-phase fragmentation chemistry: influence of glycosidic linkage position. Phys. Chem. Chem. Phys. **19**, 25643–25652 (2017)
43. Bythell, B.J., Abutokaikah, M.T., Wagoner, A.R., Guan, S., Rabus, J.M.: Cationized carbohydrate gas-phase fragmentation chemistry. J. Am. Soc. Mass Spectrom. **28**, 688–703 (2017)
44. Hofmeister, G.E., Zhou, Z., Leary, J.A.: Linkage position determination in lithium-cationized disaccharides: tandem mass spectrometry and semi-empirical calculations. J. Am. Chem. Soc. **113**, 5964–5970 (1991)
45. Cancilla, M.T., Penn, S.G., Carroll, J.A., Lebrilla, C.B.: Coordination of alkali metals to oligosaccharides dictates fragmentation behavior in matrix assisted laser desorption ionization/Fourier transform mass spectrometry. J. Am. Chem. Soc. **118**, 6736–6745 (1996)
46. Tsai, S.-T., Chen, J.-L., Ni, C.-K.: Does low-energy collision-induced dissociation of lithiated and sodiated carbohydrates always occur at anomeric carbon of the reducing end? Rapid Commun. Mass Spectrom. **31**, 1835–1844 (2017)
47. Chen, J.-L., Nguan, H.S., Hsu, P.-J., Tsai, S.-T., Liew, C.Y., Kuo, J.-L., Hu, W.-P., Ni, C.-K.: Collision-induced dissociation of sodiated glucose and identification of anomeric configuration. Phys. Chem. Chem. Phys. **19**, 15454–15462 (2017)
48. Domon, B., Costello, C.E.: A systematic nomenclature for carbohydrate fragmentations in FAB-MS/MS spectra of glycoconjugates. Glycoconj. J. **5**, 397–409 (1988)
49. Khanal, N., Masellis, C., Kamrath, M.Z., Clemmer, D.E., Rizzo, T.R.: Glycosaminoglycan analysis by cryogenic messenger-tagging IR spectroscopy combined with IMS-MS. Anal. Chem. **89**, 7601–7606 (2017)
50. Masellis, C., Khanal, N., Kamrath, M.Z., Clemmer, D.E., Rizzo, T.R.: Cryogenic vibrational spectroscopy provides unique fingerprints for glycan identification. J. Am. Soc. Mass Spectrom. (2017). https://doi.org/10.1007/s13361-017-1728-6
51. Mucha, E., González Flórez, A.I., Marianski, M., Thomas, D.A., Hoffmann, W., Struwe, W.B., Hahm, H.S., Gewinner, S., Schöllkopf, W., Seeberger, P.H., von Helden, G., Pagel, K.: Glycan fingerprinting using cold-ion infrared spectroscopy. Angew. Chem. Int. Ed. **56**, 11248–11251 (2017)
52. Mucha, E., Lettow, M., Marianski, M., Thomas, D.A., Struwe, W.B., Harvey, D.J., Meijer, G., Seeberger, P.H., von Helden, G., Pagel, K.: Fucose migration in intact protonated glycan ions - a universal phenomenon in mass spectrometry. Angew. Chem. Int. Ed. **0**. https://doi.org/10.1002/anie.201801418
53. Schindler, B., Barnes, L., Renois, G., Gray, C., Chambert, S., Fort, S., Flitsch, S., Loison, C., Allouche, A.-R., Compagnon, I.: Anomeric memory of the glycosidic bond upon fragmentation and its consequences for carbohydrate sequencing. Nat. Commun. **8**(973), (2017). https://doi.org/10.1038/s41467-017-01179-y
54. Renois-Predelus, G., Schindler, B., Compagnon, I.: Analysis of sulfate patterns in glycosaminoglycan oligosaccharides by MSn coupled to infrared ion spectroscopy: the case of GalNAc4S and GalNAc6S. J. Am. Soc. Mass Spectrom. (2018). https://doi.org/10.1007/s13361-018-1955-5
55. Barnes, L., Schindler, B., Chambert, S., Allouche, A.-R., Compagnon, I.: Conformational preferences of protonated N-acetylated hexosamines probed by InfraRed multiple photon dissociation (IRMPD) spectroscopy and ab initio calculations. Int. J. Mass Spectrom. **421**, 116–123 (2017)
56. Bakker, J.M., Besson, T., Lemaire, J., Scuderi, D., Maître, P.: Gas-phase structure of a π-allyl−palladium complex: efficient infrared spectroscopy in a 7 T Fourier transform mass spectrometer. J. Phys. Chem. A. **111**, 13415–13424 (2007)
57. Prazeres, R., Glotin, F., Insa, C., Jaroszynski, D.A., Ortega, J.M.: Two-colour operation of a free-electron laser and applications in the mid-infrared. Eur. Phys. J. At. Mol. Opt. Plasma Phys. **3**, 87–93 (1998)
58. Lemaire, J., Boissel, P., Heninger, M., Mauclaire, G., Bellec, G., Mestdagh, H., Simon, A., Caer, S.L., Ortega, J.M., Glotin, F., Maitre, P.: Gas phase infrared spectroscopy of selectively prepared ions. Phys. Rev. Lett. **89**, 273002 (2002)
59. Supady, A.: adrianasupady/fafoom, https://github.com/adrianasupady/fafoom
60. Marianski, M., Supady, A., Ingram, T., Schneider, M., Baldauf, C.: Assessing the accuracy of across-the-scale methods for predicting carbohydrate conformational energies for the examples of glucose and α-maltose. J. Chem. Theory Comput. **12**, 6157–6168 (2016)
61. Supady, A., Blum, V., Baldauf, C.: First-principles molecular structure search with a genetic algorithm. J. Chem. Inf. Model. **55**, 2338–2348 (2015)
62. Halgren, T.A.: Merck molecular force field. I. Basis, form, scope, parameterization, and performance of MMFF94. J. Comput. Chem. **17**, 490–519 (1996)

63. Halgren, T.A.: Merck molecular force field. II. MMFF94 van der Waals and electrostatic parameters for intermolecular interactions. J. Comput. Chem. **17**, 520–552 (1996)
64. Halgren, T.A.: Merck molecular force field. III. Molecular geometries and vibrational frequencies for MMFF94. J. Comput. Chem. **17**, 553–586 (1996)
65. Halgren, T.A., Nachbar, R.B.: Merck molecular force field. IV. Conformational energies and geometries for MMFF94. J. Comput. Chem. **17**, 587–615 (1996)
66. Halgren, T.A.: Merck molecular force field. V. Extension of MMFF94 using experimental data, additional computational data, and empirical rules. J. Comput. Chem. **17**, 616–641 (1996)
67. Frisch, M.J., Trucks, G.W., Schlegel, H.B., Scuseria, G.E., Robb, M.A., Cheeseman, J.R., Scalmani, G., Barone, V., Mennucci, B., Petersson, G.A., Nakatsuji, H., Caricato, M., Li, X., Hratchian, H.P., Izmaylov, A.F., Bloino, J., Zheng, G., Sonnenberg, J.L., Hada, M., Ehara, M., Toyota, K., Fukuda, R., Hasegawa, J., Ishida, M., Nakajima, T., Honda, Y., Kitao, O., Nakai, H., Vreven, T., Montgomery, J.A., Peralta, J.E., Ogliaro, F., Bearpark, M., Heyd, J.J., Brothers, E., Kudin, K.N., Staroverov, V.N., Kobayashi, R., Normand, J., Raghavachari, K., Rendell, A., Burant, J.C., Iyengar, S.S., Tomasi, J., Cossi, M., Rega, N., Millam, J.M., Klene, M., Knox, J.E., Cross, J.B., Bakken, V., Adamo, C., Jaramillo, J., Gomperts, R., Stratmann, R.E., Yazyev, O., Austin, A.J., Cammi, R., Pomelli, C., Ochterski, J.W., Martin, R.L., Morokuma, K., Zakrzewski, V.G., Voth, G.A., Salvador, P., Dannenberg, J.J., Dapprich, S., Daniels, A.D., Farkas, Foresman, J.B., Ortiz, J.V., Cioslowski, J., Fox, D.J.: Gaussian 09, Revision E.01. Gaussian, Inc., Wallingford (2009)
68. Lee, C., Yang, W., Parr, R.G.: Development of the Colle-Salvetti correlation energy formula into a functional of the electron density. Phys. Rev. B. **37**, 785–789 (1988)
69. Stephens, P.J., Devlin, J.F., Chabalowski, C.F., Frisch, M.J.: Ab initio calculation of vibrational absorption and circular dichroism spectra using density functional force fields. J. Phys. Chem. **98**, 11623–11627 (1994)
70. Becke, A.D.: Density-functional thermochemistry. III. The role of exact exchange. J. Chem. Phys. **98**, 5648–5652 (1993)
71. Zhao, Y., Schultz, N.E., Truhlar, D.G.: Exchange-correlation functional with broad accuracy for metallic and nonmetallic compounds, kinetics, and noncovalent interactions. J. Chem. Phys. **123**(16), 161103 (2005)
72. Zhao, Y., Truhlar, D.G.: The M06 suite of density functionals for main group thermochemistry, thermochemical kinetics, noncovalent interactions, excited states, and transition elements: two new functionals and systematic testing of four M06-class functionals and 12 other functionals. Theor. Chem. Accounts. **120**, 215–241 (2008)
73. Møller, C., Plesset, M.S.: A note on an approximation treatment for many-electron systems. Phys. Rev. E. **46**, 618–622 (1934)
74. Lifshitz, C.: Chem. Soc. Rev. **30**, 186–192 (2001)
75. Gilbert, R.G., Smith, S.C. (1990) Theory of unimolecular and recombination reactions. Blackwell Scientific Publications.
76. Beyer, T., Swinehart, D.F.: Algorithm 448: number of multiply-restricted partitions. Commun. ACM. **16**, 379 (1973)
77. Gritsenko, O.V., Ensing, B., Schipper, P.R.T., Baerends, E.J.: Comparison of the accurate Kohn-Sham solution with the generalized gradient approximations (GGAs) for the SN2 reaction F- + CH3F -> FCH3 + F-: a qualitative rule to predict success or failure of GGAs. J. Phys. Chem. A. **104**, 8558–8565 (2000)
78. Laerdahl, J.K., Uggerud, E.: Gas phase nucleophilic substitution. Int. J. Mass Spectrom. **214**, 277–314 (2002)
79. Bleiholder, C., Paizs, B.: Competing gas-phase fragmentation pathways of asparagine-, glutamine-, and lysine-containing protonated dipeptides. Theor. Chem. Accounts. **125**, 387–396 (2010)
80. Bythell, B.J., Harrison, A.G.: Formation of a_1 ions directly from oxazolone b_2 ions: an energy-resolved and computational study. J. Am. Soc. Mass Spectrom. **26**, 774–781 (2015)
81. Bythell, B.J., Barofsky, D.F., Pingitore, F., Polce, M.J., Wang, P., Wesdemiotis, C., Paizs, B.: Backbone cleavages and sequential loss of carbon monoxide and ammonia from protonated AGG: a combined tandem mass spectrometry, isotope labeling, and theoretical study: supporting information. J. Am. Soc. Mass Spectrom. **18**, 1291–1303 (2007)